AADE-22-FTCE-008

CFD Modeling of Flow Channels in Non-Newtonian Wellbores with Drill Pipe Rotation

David Rathgeber, Dr. Lee Richards, Montana Tech; Dr. Erick Johnson and Dr. Ryan Anderson, Montana State University

Abstract

Extended reach drilling (ERD) projects are becoming increasingly common, but pose unique challenges regarding cuttings transport. It is often not possible to use low viscosity fluids that are conducive to achieving turbulent flow conditions due to the need for additives required for barite suspension. Therefore, high-side fluid channeling can result from laminar flow conditions in many high-angle drilling situations. By modeling the fluid flow in these wellbores using Computational Fluid Dynamic (CFD) software, patterns of fluid channeling can be identified in hopes of recognizing cuttings transport inefficiencies.

Using Siemens STAR CCM+ 2020.2.1, a horizontal 12.25" wellbore model was constructed using a 5.5" drill string to simulate real-world ERD high-angle and tangent section hole conditions, where cuttings transport issues often arise. Four drilling fluid models were used to simulate typical water and oil-based drilling fluids and analyzed against 3 drill pipe eccentricities, 4 internal pipe rotation speeds (0, 60, 120, 180 rpm) and 2 flow velocities (100 ft/min and 200 ft/min) to quantify the sensitivity of each variable. Drilling fluid rheology was modeled using the Hershel-Buckley method. Axial and rotational flow regimes are both present in horizontal drilling operations; these forces are coupled in non-Newtonian flow and were modeled accordingly.

This work provides a greater understanding of the parameters that affect flow channeling and will lead to more optimal hole cleaning methods for drilling operations. In addition, this model provides a template for implementing multiphase flow regimes which include cuttings to further evaluate drilling parameter manipulation for cuttings transport optimization.

Introduction

In extended reach drilling applications, ensuring adequate hole cleaning is a critical component to efficient drilling operations, as well as reducing overall operational risk. Cuttings transport becomes increasingly difficult as wellbore inclination increases. Several previous studies identifying the fundamentals of hole angle effects on cuttings transport (Sifferman and Becker 1992)(Peden, Ford, and Oyeneyin 1990) highlighted that cuttings management challenges change at different inclinations. In high-angle wellbores (65°+) gravitational effects result in both cuttings and drill pipe settling on the bottom of the wellbore. Although turbulent flow is ideal in high inclination wellbores, thin rheology drilling fluids are often impractical due to the need to suspend weighting agents to control density. Therefore, flow is more often laminar, causing fluid channeling on the high-side of the wellbore.

In order to counteract reduced cuttings transport efficiencies caused by high-angle wellbores, operators often modify operating parameters. A 2010 experimental study by Nazari et.al. (Nazari, Hareland, and Azar 2010) compared a range of variables that can affect hole cleaning efficiency. They identified that hole size and angle have a significant effect on hole cleaning; variables that are commonly part of drilling programs, particularly in extended reach horizontal wells.

In ERD applications, large hole diameter (often 12 ¼"+) wellbores are often seen in intermediate, tangent and even production-hole sections (80°-90° inclination). This often leads to significant hole cleaning challenges due to high cuttings volume and high flow rate requirements to achieve optimal fluid velocities of 200 feet/minute (1000 gallons per minute) or more. Additionally, the extended length of these tangent sections (Chayvo Field Northern Russia has a range of tangent sections exceeding 4km, (Gupta et al. 2014)) reduces the size of cuttings through steady grinding against the drill pipe, making carrying cuttings out of the hole more difficult. Several studies, summarized in a recent report by Pedrosa et.al. (Pedrosa, Saasen, and Ytrehus 2021), indicate that as wellbore inclination increases, cuttings size tends to diminish, leading to different cuttings transport mechanism requirements. The primary mechanism for larger cuttings is convective transport in the axial direction, mainly influenced by flow rate. However, small diameter cuttings settle on the floor of the wellbore into a more tightly packed configuration. Cohesive forces increase between the grains, and higher shear stresses are then required to lift and move the cuttings. This leads to increased cuttings bed size, resulting in higher torque and drag, ECD and risk of stuck pipe (Pedrosa et al. 2021).

In these ERD tangent sections, it is often not possible to achieve industry recommended flow rates (200+ ft/min) due to tight drilling margins or equipment capabilities. Operators often look at other areas to increase hole cleaning efficiency. Drill pipe rotation can effectively help increase cuttings transport efficiency in horizontal wellbores by stirring up

cuttings from the low-side of the annulus, allowing transport in high-side fluid channels. Additionally, in large annuli, where the pipe to hole area ratio (P-HAR) exceeds 3.25 (labeled "big-hole")(Mims, Krepp, and Williams 2007), a sudden increase in cuttings transport efficiency has been observed in the field at the 120RPM range (and although less pronounced, again at the 180 RPM range). Although this phenomenon is recognized, it has not been observed in an experimental setting. There are currently no experimental flow loops specifically designed to replicate high-angle, large wellbore drilling conditions where this step change in cuttings transport efficiency is observed.

$$P - HAR = \frac{R_h^2}{R_p^2} \quad (1)$$

Our comparative study evaluates the effects of drill pipe rotation speed and fluid rheology on fluid channeling in PHAR-identified "big-hole" scenarios. Additionally, we aim to identify potential causes of the industry-recognized step change at the 120RPM and 180RPM range. Our results are based from results of a three-dimensional (3D), single-phase, coupled, steady-state CFD model of a horizontal, 12 ¼" annulus using Siemens STAR CCM+® software. Drilling fluid properties are modeled using rheometer data collected from a previous design study (Rathgeber 2019). Herschel-Bulkley (modified power law) is used to model the shear thinning properties of drilling fluid and SST K-Omega turbulence modeling is used estimate model turbulence between the rotating pipe wall and flow stream.

Model Set Up

In order to accurately model wellbore sections that promote the cuttings transport "step change" seen in big hole, this model design is based on large-diameter, high-angle wellbores often seen in extended reach drilling applications. 12.25" ID annuli are often seen in intermediate and tangent sections (Wytch Farm-BP, Chayvo Field-Rosneft, Liuhua Field-CNOOC), and occasionally in oversized production-hole sections. This large-diameter wellbore is classified as "big hole" by P-HAR (EQ) calculations (>3.25) when drilling with any drill string with a nominal OD equal to or less than 6.625".

Wellbore and Pipe Parameters

The fluid volume section of this model consists of a horizontal 12.25" ID horizontal wellbore measuring 744" (62 feet). The internal drill string is a 5.5" OD pipe body with a centrally located 5.75" by 24" OD tool joint. In order to more closely replicate wall boundary conditions, surface roughness height of the drill pipe is set to 0.0018" (typical roughness for steel pipe) and wellbore wall surface roughness height is comparable to dolomite rock at 0.12".

The internal drill pipe for our models consist of 3 different eccentricities, to simulate actual downhole conditions. As a baseline, a drill pipe centered within the annulus is used to model concentric flow. A second eccentric model places the drill string on the low side of the wellbore, simulating pipe resting near the wellbore floor. A third model simulates a slightly offset pipe, simulating "pipe-walk" – the act of the pipe rolling up the side of the wellbore at high RPM.

As these models are steady-state in nature, all drill string models rotate on their local axis, with no axisymmetric motion. The distance from the wellbore wall in the eccentric models is 1.75" from the pipe body, and 1" from the tool joint.

Fluid Properties

Exploration & Production (E&P) operators often utilize a range of drilling fluids dependent on expected wellbore conditions and performance metrics. These fluids can be water-based (WBM) or oil-based (OBM), with modified densities and rheological properties related to wellbore formation pressures and cuttings transport characteristics. This research compares four separate drilling fluids whose rheometer measurements are outline in Table 1

. From this field data, values for yield point *YP* (2), plastic viscosity *PV* (3), Shear Stress, τ_y (4) power law exponent *n* (5) and consistency factor *K* (6) were calculated (utilizing a rheometer field viscometer shear rate correction factor of 1,066) for input into the CFD software (Table 2).

.

$$YP = RPM\ 600° - RPM\ 300° \quad (2)$$

$$YP = RPM\ 300° - PV \quad (3)$$

$$\tau_y = 2\frac{RPM\ 3°}{1.066} - \frac{RPM\ 6°}{1.066} \quad (4)$$

$$n = 3.32\log\left(\frac{\frac{RPM\ 600°}{1.066} - \frac{\tau_y}{1.066}}{\frac{RPM\ 300°}{1.066} - \tau_y}\right) \quad (5)$$

$$K = \left(\frac{\frac{RPM\ 300°}{1.066} - \tau_y}{511^n}\right) \times 1.066 \quad (6)$$

Fluid Modeling Properties

Although the rheological parameters of drilling fluids can be affected by both temperature and pressure gradients in drilling operations, we assume in this study isothermal and isobaric conditions. Drilling fluids have non-Newtonian, shear thinning properties. Although there are several methods for modeling non-Newtonian fluids (Power Law, Bingham-Plastic), API RP13D highlights the Herschel-Bulkley method for characterizing the shear thinning properties of drilling fluid in wellbores (7).

$$\tau = \tau_0 + K_{\dot{\gamma}^n} \quad (7)$$

Although drilling fluid flow is primarily laminar due to rheological properties, there is expected to be some turbulent and transitional flow near the rotating pipe boundary, particularly as RPM's increase. To effectively model this flow regime change, the SST (Shear Stress Transport) K-Omega turbulence model is utilized. This model is a combination of the K-Epsilon turbulence model, which is effective for modeling free-stream turbulence (that may be encountered in annular flow) and the K-Omega turbulence model, which more accurately describes flow turbulence at the pipe wall. The SST model design switches from K-Omega to K-Epsilon

The drilling fluid in all simulations is treated as incompressible, with a constant density. Fluid flow physics are calculated utilizing coupled flow equations, solving all unknowns in a coupled equation per iteration. Gravity parameters are set to -32.2 ft/sec^2 to simulate gravitational forces on the horizontal wellbore.

Mesh Parameters

In order to ensure adequate model resolution, a 1" mesh base size per element is selected with a minimum surface size of 20% relative to the base (0.2"). This resolution allows for acceptably converged solutions. As both the wellbore and drill string are cylindrical in nature, the generalized cylinder mesh is utilized to ensure rounded surfaces are modeled appropriately, with one element per 6°. In order to optimize the SST K-Omega turbulence model, a prism layer mesh consisting of 4 layers is utilized, with a growth rate of 1.4.

Detailed mesh parameters can be found in Table 3.

Results

Visual cross-sections of all simulation runs are recorded at approximately 43 feet from the inlet. This location is chosen to eliminate any inlet effects seen early in flow development (Figure 1). Additionally, it is approximately 11 feet from the modeled drill string tool joint, where tighter wellbore geometry temporarily increases flow velocity.

At this cross-sectional area, both normal and absolute velocity segments are evaluated. "Normal" velocity cross-sections show the velocity component perpendicular to the inlet (straight along the wellbore axis) in the wellbore. The result is a clear visual representation of directional flow channel location, area and magnitude. This normal flow channel is a primary driver for removing cuttings from the wellbore in high-angle sections, transporting cuttings along the wellbore axis to the surface.

"Absolute" velocity cross-sections identify the total velocity magnitude, regardless of direction (Figure 2 shows the vector difference between normal and absolute flow).

As pipe rotation speed increases, these numbers are often larger than the normal flow, as effects from the rotating pipe on fluid increases, particularly near the pipe wall. These values are important on the bottom half of the wellbore, where smaller cuttings tend to settle into tightly consolidated beds, with cohesive effects binding cuttings to each other and the wellbore wall. This increased cohesion requires higher velocities to break cohesive forces and transport as individual particles. Due to high-side fluid channeling, higher normal velocities often do not reach the cuttings beds.

100 Feet Per Minute (FPM) Linear Velocity

Half of flow models (48 simulations) were created using an inlet flow rate matching a linear velocity of 100 fpm (1.667 ft/sec). This velocity is half the industry recommended rate of 200 fpm (3.3 ft/sec) for optimal hole cleaning. At this size of wellbore (12.25"), the pump rate required to achieve 200 fpm linear velocity is approximately 500 gallons per minute (gpm).

Pipe Eccentricity Effects on Channel Development

Visual data collected from simulations based on pipe location without drill pipe rotation show that flow channel development is more pronounced in simulations with eccentric pipe locations, with maximum flow channel velocity nearing 150 fpm (2.5 ft/sec). Centrally located pipe shows minimal flow channel development, with an even distribution of flow around the drill pipe. This results in minimal velocity change, with highest observed linear velocity being approximately 130 fpm (2.15 ft/sec). Figure 3 shows a direct comparison of flow channel development by pipe eccentricity for LOBM.

In bottom-eccentric simulations, the flow channeling is located in the top half of the wellbore, with bottom-half linear velocity ranging from 60 to 90 fpm (1-1.5 ft/sec). In offset-eccentric simulations, the flow channel is shifted in the direction of the open wellbore, with partial flow channel distribution in the bottom half of the annulus. Figure 4 shows bottom-half flow velocity contour comparison of bottom and offset pipe eccentric simulations from LOBM.

In comparing cross-sections between fluid rheology models, flow channel development becomes slightly more developed from light rheology fluids (LOBM, LWBM) to thicker, more dense rheology fluids (MOBM, MWBM), with maximum linear velocity increasing by approximately 5 fpm. This minor increase in maximum velocity has a negligible effect on channel size or distribution. Figure 5 shows flow channel development of MOBM by pipe eccentricity at 0RPM, which can be compared with Figure 3 (LOBM).

Drill Pipe Rotation Speed Effects on Channel Development

As pipe RPM increases in all models, normal velocity decreases, indicating that the pipe rotation disrupts linear flow. More pronounced drops in linear velocity are observed in eccentric simulations, where flow channeling is more significant.

Concentric Pipe

In light-rheology fluid concentric simulations, normal velocity gradually reduces from a thin ring-shaped channel with maximum linear velocity of approximately 122 fpm (2.03 ft/sec), to a more evenly distributed flow throughout the annulus with a maximum linear velocity of 116 fpm (1.93 ft/sec) (Figure 6, LWBM) LOBM saw a larger decrease from

124 fpm (2.07 ft/sec) to 117 fpm (1.95 ft/sec). However, as normal flow decreases, absolute velocity magnitudes increase from the drill pipe wall. At 60 RPM, absolute flow differs minimally from stationary pipe values, indicating little to no effect on flow channeling. At 120 RPM, absolute flow velocity shows a steady increase in overall average velocity, with increased thickness in flow channel, growing inward towards the rotating inner pipe. At 180 RPM, absolute velocity magnitudes are largest at the drill pipe wall, reducing steadily outward to the wellbore wall (Figure 7).

In medium rheology fluids, flow channeling is more persistent, with less fluctuation in normal velocity as pipe rotation speeds increase (125 fpm [2.08 ft/sec] to 118 fpm [1.97 ft/sec] in MOBM, 114 fpm [1.9 ft/sec] to 110 fpm [1.83 ft/sec] in MWBM).

Bottom Eccentricity Pipe

In bottom-eccentric, light-rheology simulations, there is an immediate effect on flow channel absolute velocity and location as pipe RPM increases. At 0 RPM, maximum normal linear velocity magnitude is 145 fpm (2.4 ft/sec), dropping to 132 fpm (2.2 ft/sec) at 60 RPM, 126 fpm (2.1 ft/sec) at 120 RPM and 123 fpm (2.05 ft/sec) at 180 RPM (Figure 8). In addition to this reduced linear velocity, the location and spread of the flow channel immediately shifts in the direction of the pipe rotation. At the onset of pipe rotation (60 RPM), flow channel boundaries are found below the drill pipe, with decreasing velocity as pipe RPM increases.

At 60 RPM, the absolute velocity is dominated by normal flow, with contours showing similar flow channel location and magnitude. The onset of rotation does lower maximum observed velocity within the annulus, at a magnitude of approximately 15 fpm (0.25 ft/sec) across all fluids. At 120 RPM, absolute velocity magnitudes begin to increase around the entirety of the drill pipe with average velocity magnitude surpassing 125 fpm (2.08 ft/sec) below the drill pipe and along the wellbore floor. At 180 RPM, highest magnitudes are found along the wellbore floor, with velocity's exceeding 150 fpm (2.5 ft/sec) near the pipe wall (Figure 9). Similar conditions are observed with medium rheology fluids (MOBM, MWBM).

Offset Eccentricity Pipe

Similar to bottom-eccentric simulations, there is an immediate effect on the distribution and magnitude of the flow channel with the onset of pipe rotation. At 0 RPM, maximum flow channel velocity peak at 150 fpm (2.5 ft/sec) for LOBM and 147 fpm (2.45 ft/sec) for LWBM, with a pronounced channel contour within the open annular cavity. At 60 RPM, a decrease of approximately 11 fpm (139 fpm – LOBM, 136 fpm – LWBM) in maximum channel velocity is recorded, and distribution of the flow channel begins grow around the outside of the wellbore, with lower outer-channel velocities observed along the wellbore floor. At 120 RPM, a significantly smaller decrease in channel velocities are observed (3 fpm to 136 fpm - LOBM and 2 fpm to 134 fpm- LWBM) with an increased distribution of the channel in the direction of pipe rotation. At 180 RPM, maximum channel velocity remains approximately the same, but the channel distribution spreads more toward the wellbore floor. As RPM increases, the distance of the flow channel from the pipe wall increases, with the channel elongating along the wellbore wall (Figure 10).

Absolute velocity at 60 RPM shows similar contour definition as normal velocity, indicating although the flow channel position is changing, flow is predominantly still in the axial direction, with no significant centrifugal flow. Absolute maximum velocity magnitudes across all fluids see a reduction of an average of 10 fpm (0.17 ft/sec) between 0 and 60 RPM. At 120 RPM, increased fluid velocity is observed surrounding the drill pipe, but a small cavity of low velocity begins to develop on the bottom of the wellbore, opposite of the drill pipe. At 180 RPM, absolute velocities with magnitudes exceeding 250 fpm are observed near the pipe wall, particularly where pipe and wellbore wall are closest (Figure 11).

In medium-rheology fluids, similar behavior is observed, with lower velocity gradients from the pipe wall, resulting in higher velocities seen further from the wall. In addition, the cavity that developed on the wellbore wall is more clearly observed.

200 Feet Per Minute (FPM) Linear Velocity

The second half of flow models were created with an inlet flow rate matching a linear velocity of 200 fpm (3.33 ft/sec). This is the industry recommended flow rate for optimal hole cleaning – however, it is not always possible to achieve such high flow rates, due to formation fracture margins, pump capacity and downhole equipment. For 12.25" wellbores, this equates to 1000 gpm.

Effects of Fluid Velocity on Channel Development

Although the development of flow channeling remains relatively similar as flow rates increase from 100 to 200 fpm, there are several notable differences that are recorded. At lower flow rates, the onset of rotation (60 RPM) saw a reduction in absolute velocity magnitude before increasing at 120 RPM, absolute velocity values continue to decrease until 180 RPM, when absolute velocity increases. This indicates that channel creation is more dominantly controlled by flow normal to the inlet (pump rate).

At increased flow rates, flow channels see less adverse effects from pipe rotation, through both flow channel dispersion and reduced maximum velocity. Comparison of Figure 12 (200 fpm) to Figure 8 (100 fpm) show flow normal to the inlet in bottom-eccentric pipe. More pronounced flow channeling occurs at the higher flow rate, with less dispersion around the rotating pipe. In offset-eccentric pipe, one notable difference is how the flow channel tends to remain more top-centered than at lower flow rate, at the onset of pipe rotation (Figure 14 [200 fpm], Figure 10 [100 fpm]). Similarly, absolute velocity is more controlled by velocity normal to the inlet at higher flow rate in both eccentricities (Figure 13 vs Figure 9, Figure 15 vs Figure 11).

Conclusions

Review of the 96 flow simulations identifies several key observations. At increased flow rates (200 fpm), pipe rotation still effects the location of the flow channel, but absolute flow

velocity increases are more evenly distributed, with less localized high-velocity spots (Figure 9 [100 fpm] vs Figure 13 [1,000 fpm] a more even velocity distribution at higher flow rates – high velocity "hot-spot" below drill pipe at high rpm, 100 fpm).

Variable pipe eccentricity creates a fluid cavity within the top portion of the wellbore, causing flow channel development. This channeling results in centralized maximum normal velocities approximately 1.5 times higher than the linear flow rate (150 fpm channel in 100 fpm simulations, 280 fpm channel in 200 fpm simulations). Concentric (centered) drill pipe creates an evenly distributed flow pattern around the drill pipe.

The location, dispersion and maximum magnitude of developed flow channels see an immediate effect at the onset of drill pipe rotation, regardless of flow rate. As rotation begins, the channel begins to shift in the direction of pipe rotation. In addition, the centroid of the flow channel begins to disperse, losing magnitude. At 60 RPM, the highest magnitude of flow is still in the direction normal to the inlet, with minor losses in flow channel magnitude. In bottom-eccentric simulations, this allows the flow channel to reach the bottom half of the wellbore, potentially increasing cuttings bed disruption – however, in offset eccentric simulations, the flow channel is located predominantly on the top half of the wellbore.

At 120 RPM, flow channel dispersion continues in the direction of pipe rotation, with further channel centroid dispersion and reduced average velocity. In high flow rate simulations (200 fpm), maximum flow rates are still normal to the inlet. However, in low flow rate simulations (100 fpm), centrifugal flow caused by drill pipe rotation has a higher magnitude than flow normal to the inlet.

In bottom-eccentric simulations, a second channel centroid develops below the drill pipe (Figure 16). This high absolute velocity at the bottom of the wellbore could disrupt the cohesive forces encountered in dense cuttings beds, allowing for easier transport of individual cuttings. This trend is not seen in higher flow rate simulations (200 fpm).

In offset-eccentric simulations, there is no secondary channel centroid development, however a small, lower-velocity cavity appears to form between the offset flow channel and centrifugal velocity from the rotating pipe (Figure 17). This cavity is not as pronounced in higher flow rate simulations (200 fpm).

At 180 RPM and lower flow rates (100 fpm). The highest absolute velocities are observed where the drill pipe and wellbore wall are closest in proximity. This centrifugal velocity may result in cuttings transport upwards within the wellbore, as well as cause significant disruption to consolidated cuttings beds. In offset-eccentric simulations, absolute velocity magnitudes are less pronounced along the bottom of the wellbore, suggesting less disruption to cuttings beds. However, flow channel location and magnitude are more significant opposite of the rotating pipe, suggesting that the flow channel may disrupt the cuttings bed. In high flow rate simulations, flow channeling and absolute velocity magnitudes are more evenly distributed in a centrifugal manner, with the highest velocities located on the right side of the annulus (direction of drill pipe rotation). Although there are lower localized velocities along the bottom of the wellbore, the average velocity is at or above optimal hole cleaning rates (200 fpm).

CFD Model Validation

CFD model validation was performed by comparing calculated annular pressure loss (8) with simulated pressure loss, where P is annular pressure loss, MW is mud weight in ppg, L is length in feet, v is linear velocity in fpm, Dh is the hole diameter in inches, and Dp is pipe diameter in inches. Pressure losses within simulations tended to be lower than calculated pressure losses, with highest error percentage seen in LWBM. Table 4 displays calculated pressure losses and simulated pressure losses.

$$P = [(1.4327 \times 10^{-7}) \times MW \times L \times v^2] \div (Dh - Dp) \quad (8)$$

Pressure differentials vary between 6 and 36% by fluid rheology for lower flow rate calculations (100 fpm) and between 27 and 62% for higher flow rate calculations (200 fpm). This high discrepancy is due to the exponential increase in velocity between models. At time of publication, additional pressure loss methods are being tested, based on pipe eccentricity (Rushd et al. 2017).

Acknowledgments

The authors would like to thank Montana Tech and Montana State University for the collaboration and supply of CFD software for the purpose of this ongoing research.

Nomenclature

.

ERD =*Extended Reach Drilling*
CFD = *Computational Fluid Dynamics*
P-HAR =*Pipe – Hole Area Ratio*
RPM =*Revolutions Per Minute*
SST = *Shear Stress Transport*
ID = *Internal Diameter*
OD = *Outer Diameter*
E&P = *Exploration & Production*
API = *American Petroleum Institute*
RP = *Recommended Practice*
FPM = *Feet Per Minute*

Equation Variables

R_h = *Radius of wellbore, inches*
R_p = *Radius of pipe, inches*
YP = *Yield Point*
τ_y = *Shear stress*
n = *Power Law exponent*
k = *Consistency factor*
γ = *Shear rate*
CCI = *Cuttings Carrying Index*
AV = *Annular velocity, ft/min*
MW = *Mud weight, ppg*

References

Gupta, Vishwas P, Angel H P Yeap, Kyle M Fischer, Randall S Mathis, and Michael J Egan. 2014. “Expanding the Extended Reach Envelope at Chayvo Field, Sakhalin Island.” Society of Petroleum Engineers. https://doi.org/10.2118/168055-MS.

Mims, M G, A N Krepp, and H A Williams. 2007. *Drilling Design and Implementation for Extended Reach and Complex Wells*. 3rd ed. Houston: K&M Technology Group.

Nazari, T, G Hareland, and J J Azar. 2010. “Review of Cuttings Transport in Directional Well Drilling: Systematic Approach.” *SPE Western Regional Meeting*. https://doi.org/10.2118/132372-MS.

Peden, J M, J T Ford, and M B Oyeneyin. 1990. “Comprehensive Experimental Investigation of Drilled Cuttings Transport in Inclined Wells Including the Effects of Rotation and Eccentricity.” Society of Petroleum Engineers. https://doi.org/10.2118/20925-MS.

Pedrosa, Camilo, Arild Saasen, Bjørnar Lund, and Jan David Ytrehus. 2021. “Wer Drilled Cuttings Bed Rheology.” *Energies* 14 (1644): 9.

Pedrosa, Camilo, Arild Saasen, and Jan David Ytrehus. 2021. “Fundamentals and Physical Principles for Drilled Cuttings Transport - Cuttings Bed Sedimentation and Erosion.” *Energies* 14 (545): 13.

Rathgeber, David Clifford. 2019. “Horizontal Flow Loop Design for the Study of Drill String Rotation Effects on Cuttings Transport.” Montana Tech of The University of Montana.

Rushd, S., A. R. Shazed, T. Faiz, V. Kelessidis, I. G. Hassan, and A. Rahman. 2017. “CFD Simulation of Pressure Losses in Eccentric Horizontal Wells.” In *SPE Middle East Oil and Gas Show and Conference, MEOS, Proceedings*, 2017-March:287–95. Society of Petroleum Engineers (SPE). https://doi.org/10.2118/183934-ms.

Sifferman, T.R., and TE (SPE/Mobil R&D Corp) Becker. 1992. “Hole Cleaning in Full-Scale Inclined Wellbores.”

1.

Table 1: Drilling Fluid Rheometer Readings

	P Temp (F)	Rheo Temp (F)	RPM 600 (°)	RPM 300 (°)	RPM 200 (°)	RPM 100 (°)	RPM 6 (°)	RPM 3 (°)
Light WBM	75	120	47	33	27	21	12	11
Medium WBM	75	120	63	40	32	22	12	11
Light OBM	75	120	51	32	25	17	8	6
Medium OBM	75	120	74	46	35	4	0	0

Table 2: Drilling Fluid Calculated Data

	Density (ppg)	Plastic Viscosity, cP	Yield Point (lb/100ft^2)	τy	Power Law Exponent, n	Consistency Factor, K
Light WBM	9.00	14	19	9.38	0.71	0.28
Medium WBM	12.00	23	17	9.38	0.84	0.16
Light OBM	9.50	19	13	3.75	0.75	0.25
Medium OBM	12.00	28	18	7.50	0.81	0.25

Table 3: Mesh Paramters

Mesh Parameters	
Base Size	1 inch
CAD Proj	Yes
Target Surface Size (%)	150 (Relative to Base)
Min Surface Size (%)	20 (Relative to Base)
% of base	20
Abs size	0.2 inch
Surface Curvature	60 pts/circle
Max # pts per circle	360
Curvature Deviation distance	0.4 inch
Surface Proximity	
Search Floor	0 inch
# points in gap	2
Surface Growth	1.3 (Default)
Auto-Repair	0.01 (Default)
Num Prism L	4
Prism L Stretch	1.4
Prism Tot Thickness (%)	20 (relative to base)
Volume Growth rate	1.2
Max Tet Size	10000 (default)
Core Mesh O	1 (default)

Table 4: CFD Pressure Loss Calculation Comparisons

	MW (ppg)	Calculated (psi)	Simulated (psi)				
100 FPM							
			Center	Bottom	Offset	Sim Average	Avg % Difference
LOBM	9	0.118436533	0.09934672	0.1188059	0.09	0.10271754	13%
LWBM	12	0.157915378	0.09498521	0.1031194	0.10503	0.10104487	36%
MOBM	9.5	0.125016341	0.1342553	0.15888	0.160798	0.1513111	-21%
MWBM	12	0.157915378	0.7371855	0.1477728	0.1500729	0.14892285	6%
200 FPM							
			Center	Bottom	Offset	Sim Average	Avg % Difference
LOBM	9	0.473746133	0.3049292	0.3054814	0.28	0.296803533	37%
LWBM	12	0.631661511	0.2681621	0.2685934	0.18331286	0.240022787	62%
MOBM	9.5	0.500065363	0.4047231	0.4043225	0.2791367	0.362727433	27%
MWBM	12	0.631661511	0.293987	0.366186	0.366022	0.342065	46%

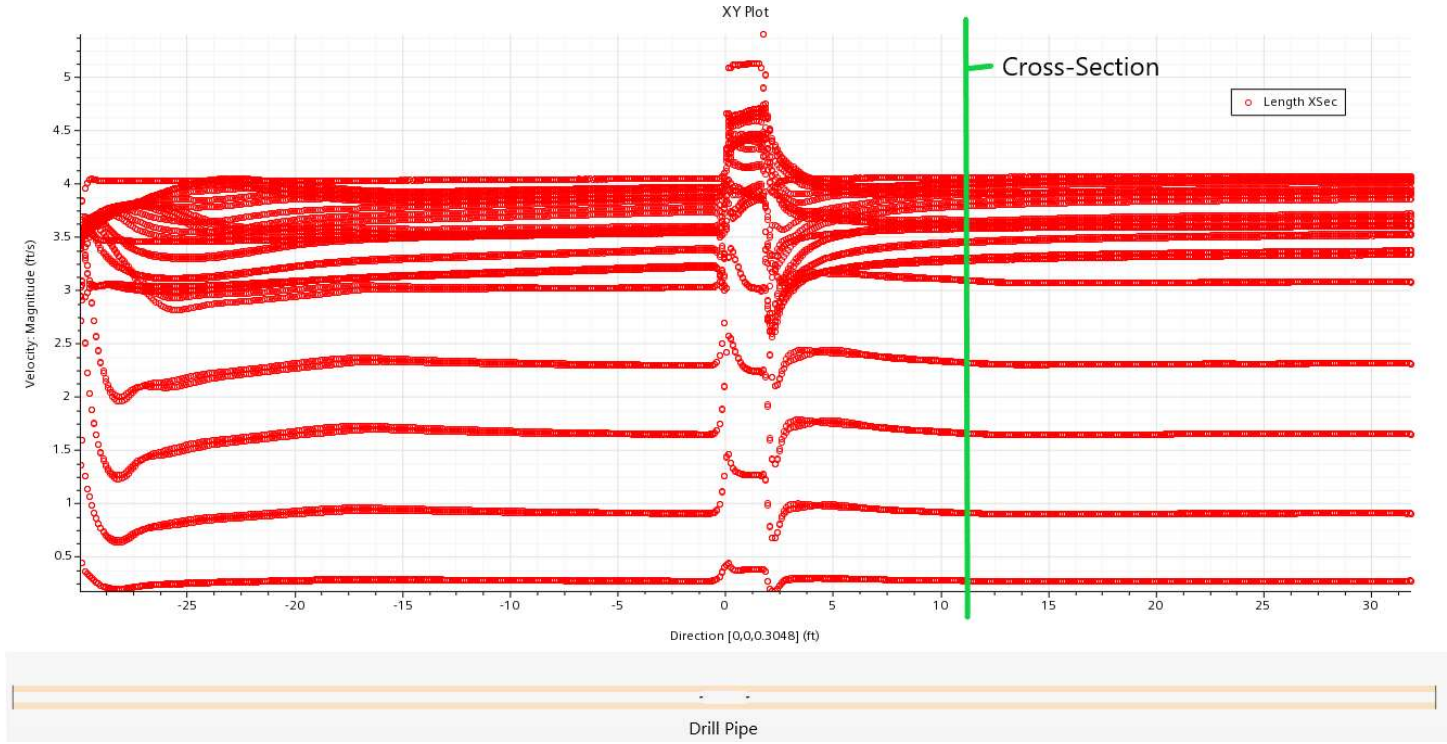

Figure 1: Axial cross section of flow model with location identification for comparative analysis

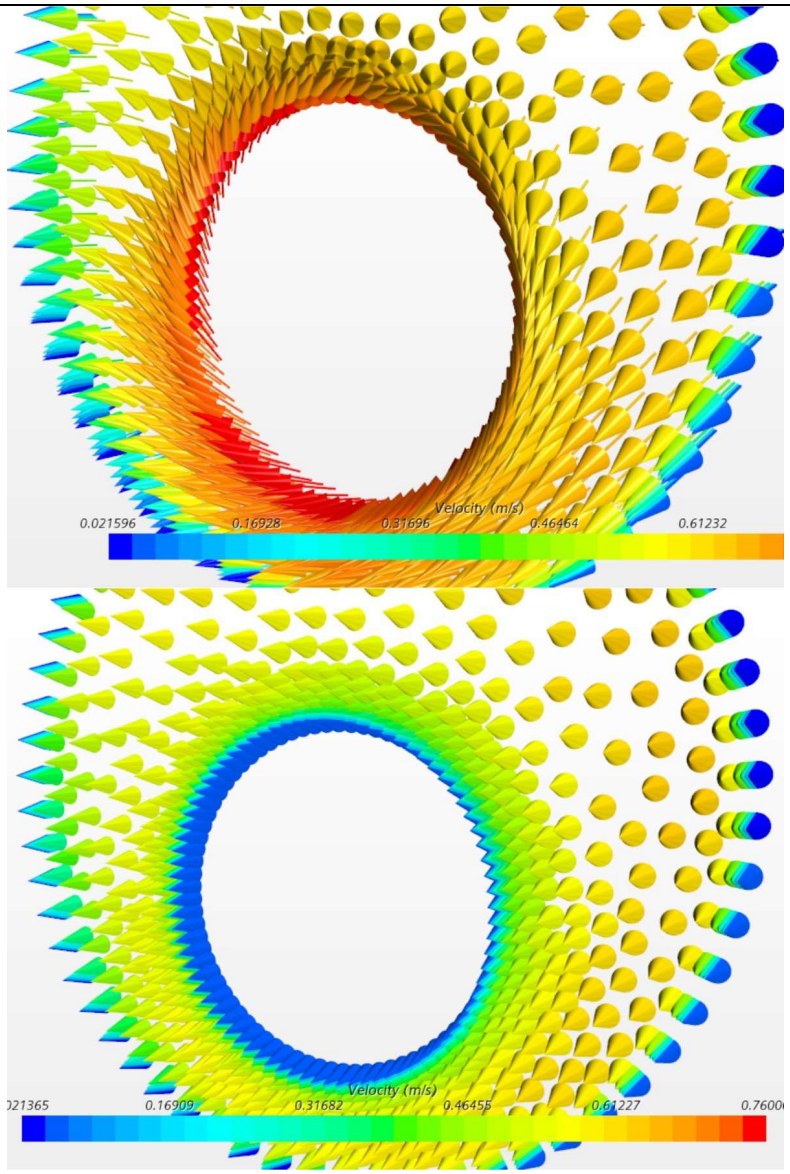

Figure 2:Comparison of "Absolute" velocity (top) to "Normal" velocity (bottom). Absolute velocity includes magnitude and direction, Normal velocity includes magnitude in the direction perpendicular to inlet

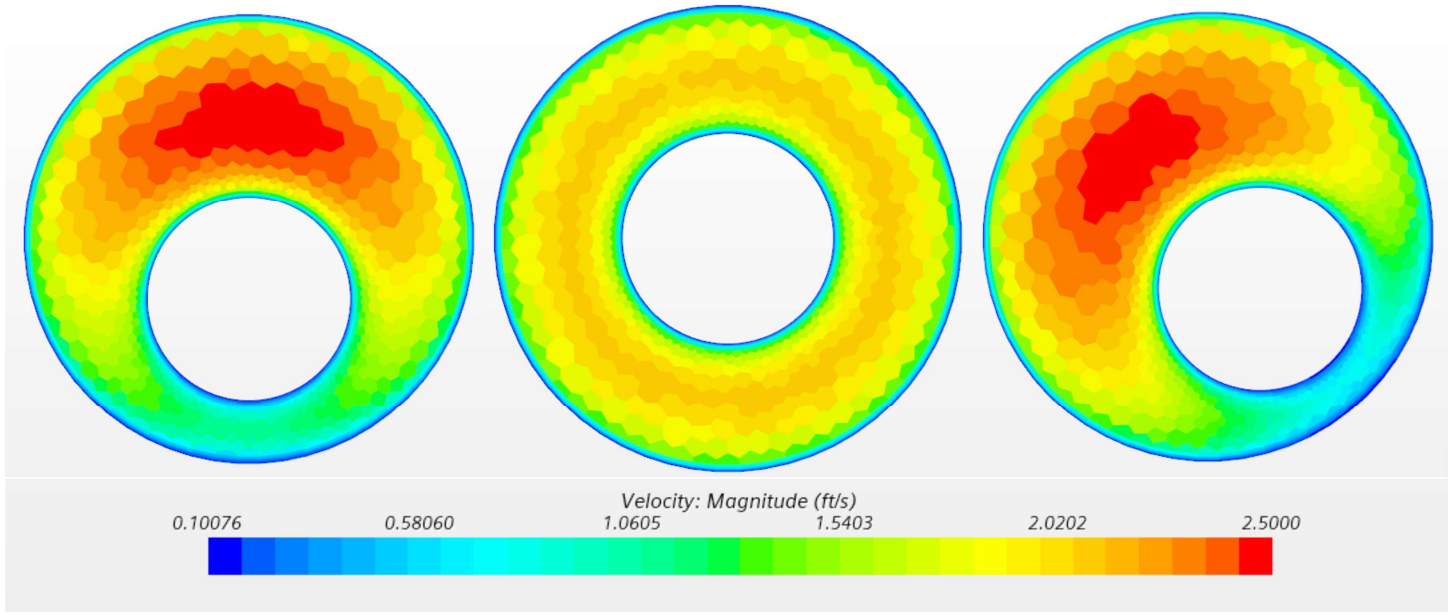

Figure 3:Cross-sectional analysis of flow channel development based on pipe eccentricity, 100 fpm linear velocity (500 gpm flow rate), LOBM

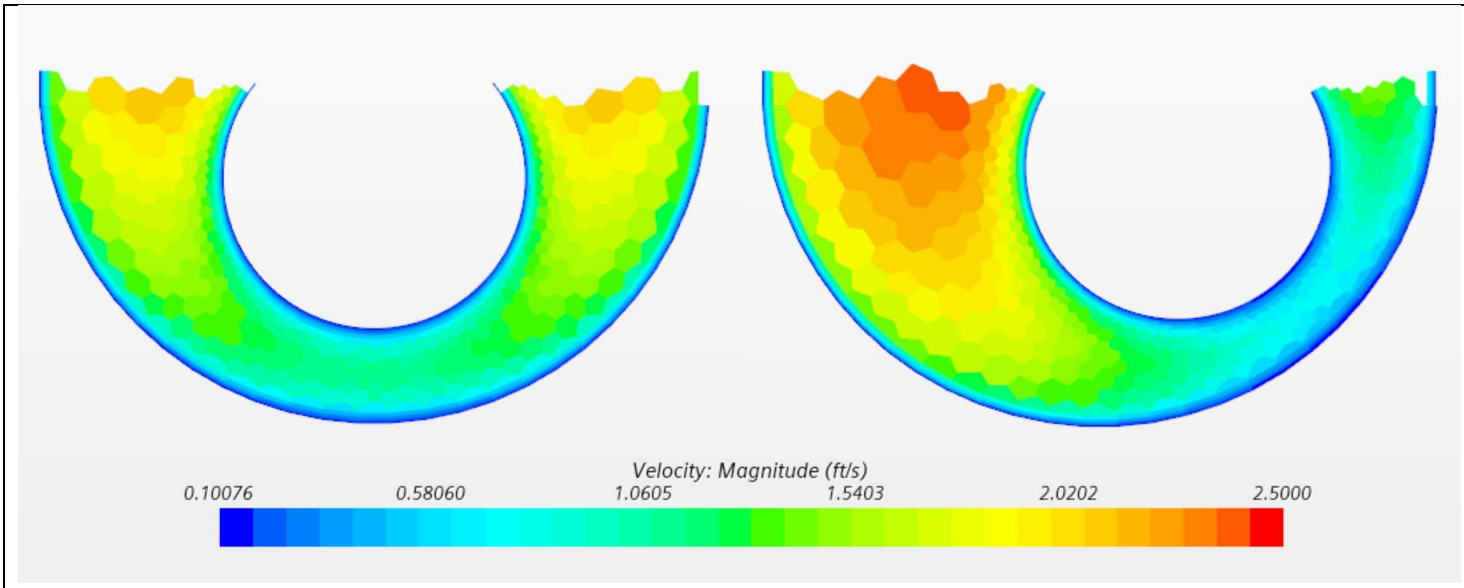

Figure 4: Cross-sectional comparison of flow channel infiltration into bottom half of wellbore by pipe eccentricity, 100 fpm linear velocity (500 gpm flow rate), LOBM

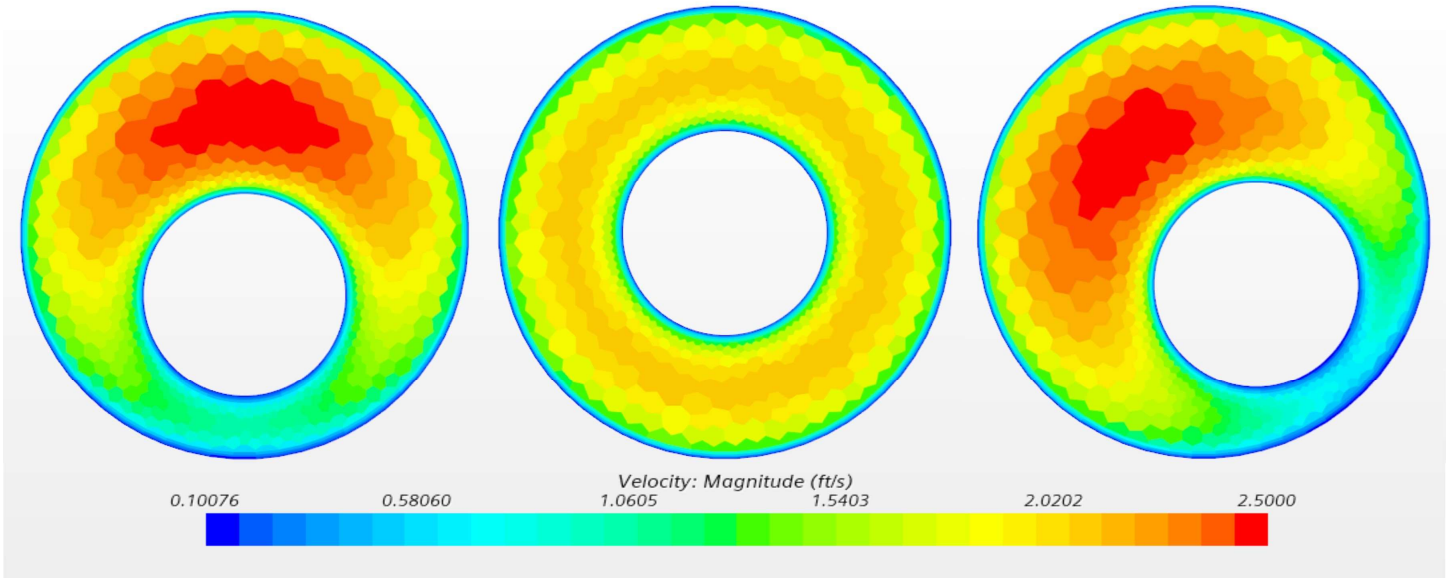

Figure 5:Cross-sectional analysis of flow channel development based on pipe eccentricity, 100 fpm linear velocity (500 gpm flow rate), MOBM

x

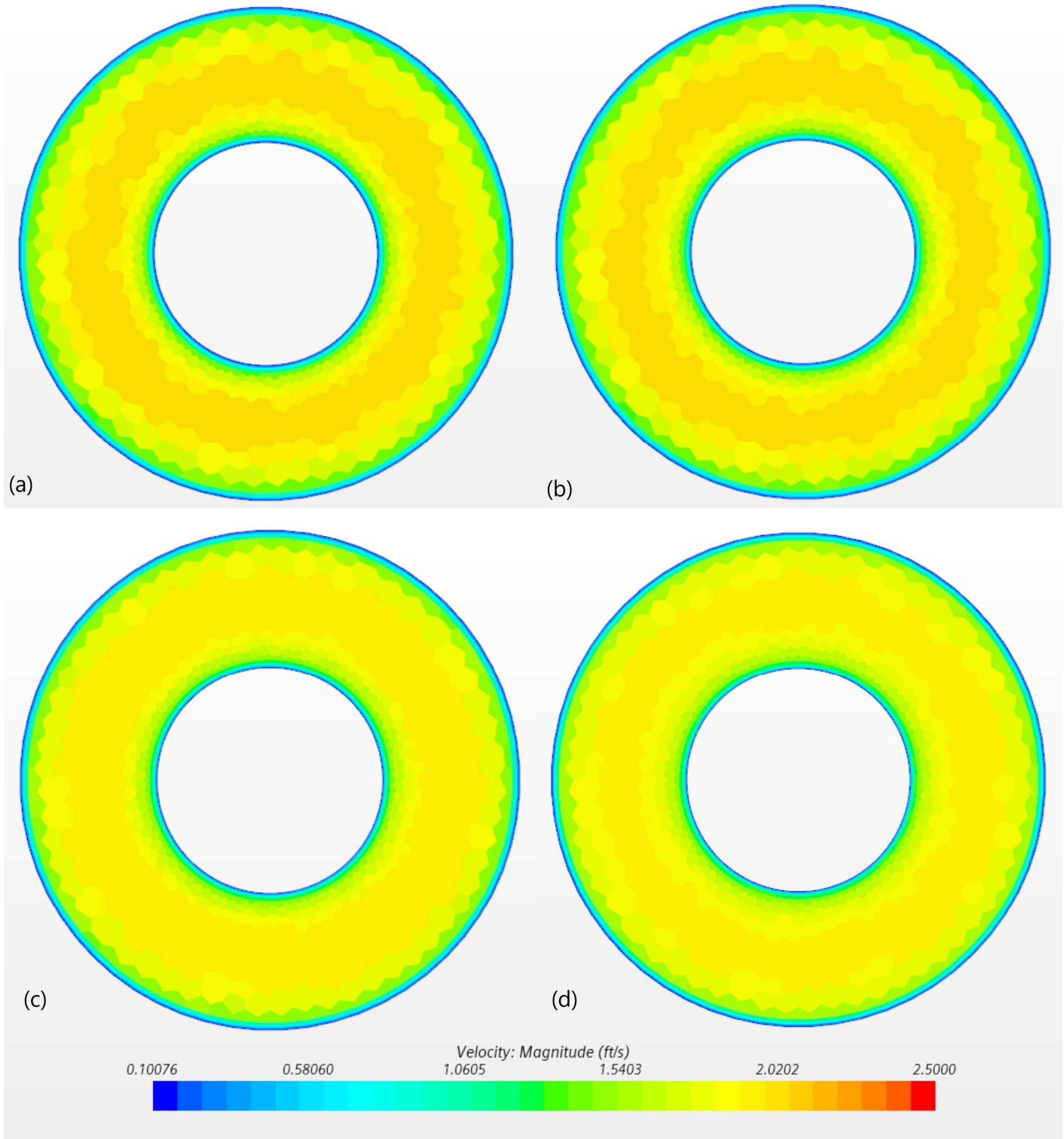

Figure 6:Cross-sectional analysis of flow channel development based on pipe rotation speed, velocity magnitude normal to inlet (100 fpm linear velocity [500 gpm flow rate], concentric annulus, LWBM) (a) 0 RPM (b) 60 RPM (c) 120 RPM (d) 180 RPM

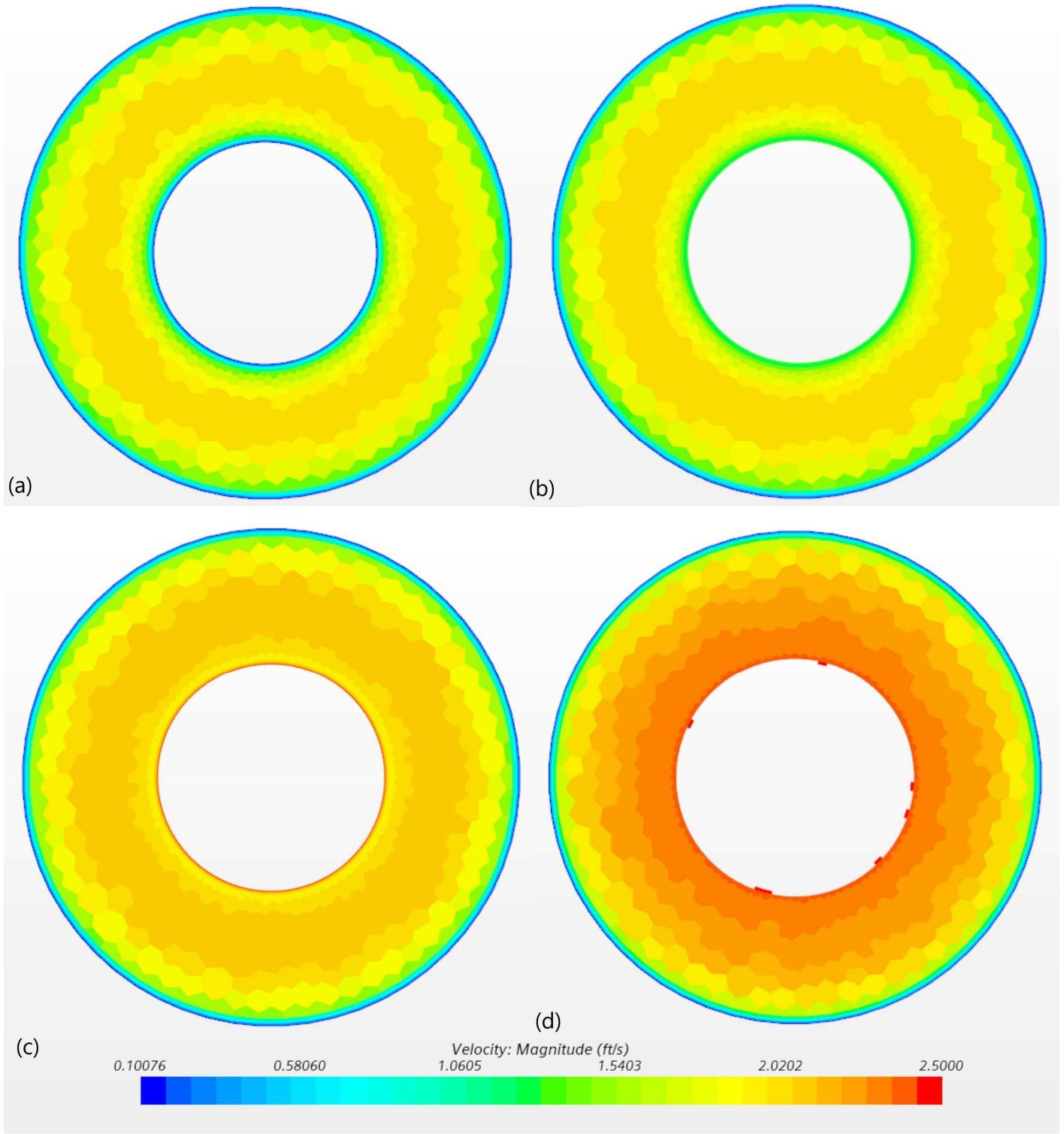

Figure 7:Cross-sectional analysis of flow channel development based on pipe rotation speed, absolute velocity magnitude (100 fpm linear velocity [500 gpm flow rate], concentric annulus, LWBM) (a) 0 RPM (b) 60 RPM (c) 120 RPM (d) 180 RPM

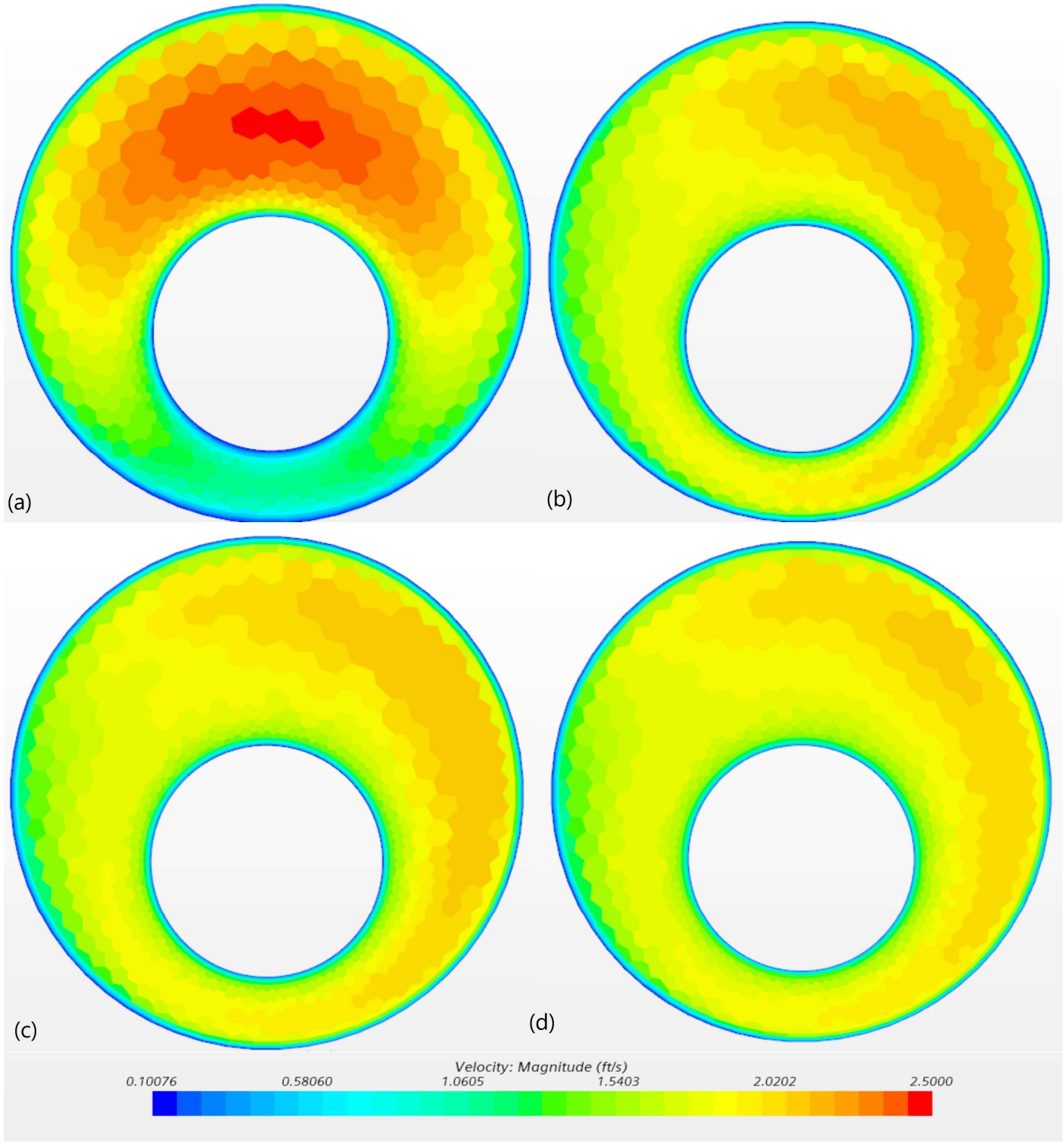

Figure 8:Cross-sectional analysis of flow channel development based on pipe rotation speed, velocity magnitude normal to inlet (100 fpm linear velocity [500 gpm flow rate], bottom eccentric annulus, LWBM) (a) 0 RPM (b) 60 RPM (c) 120 RPM (d) 180 RPM

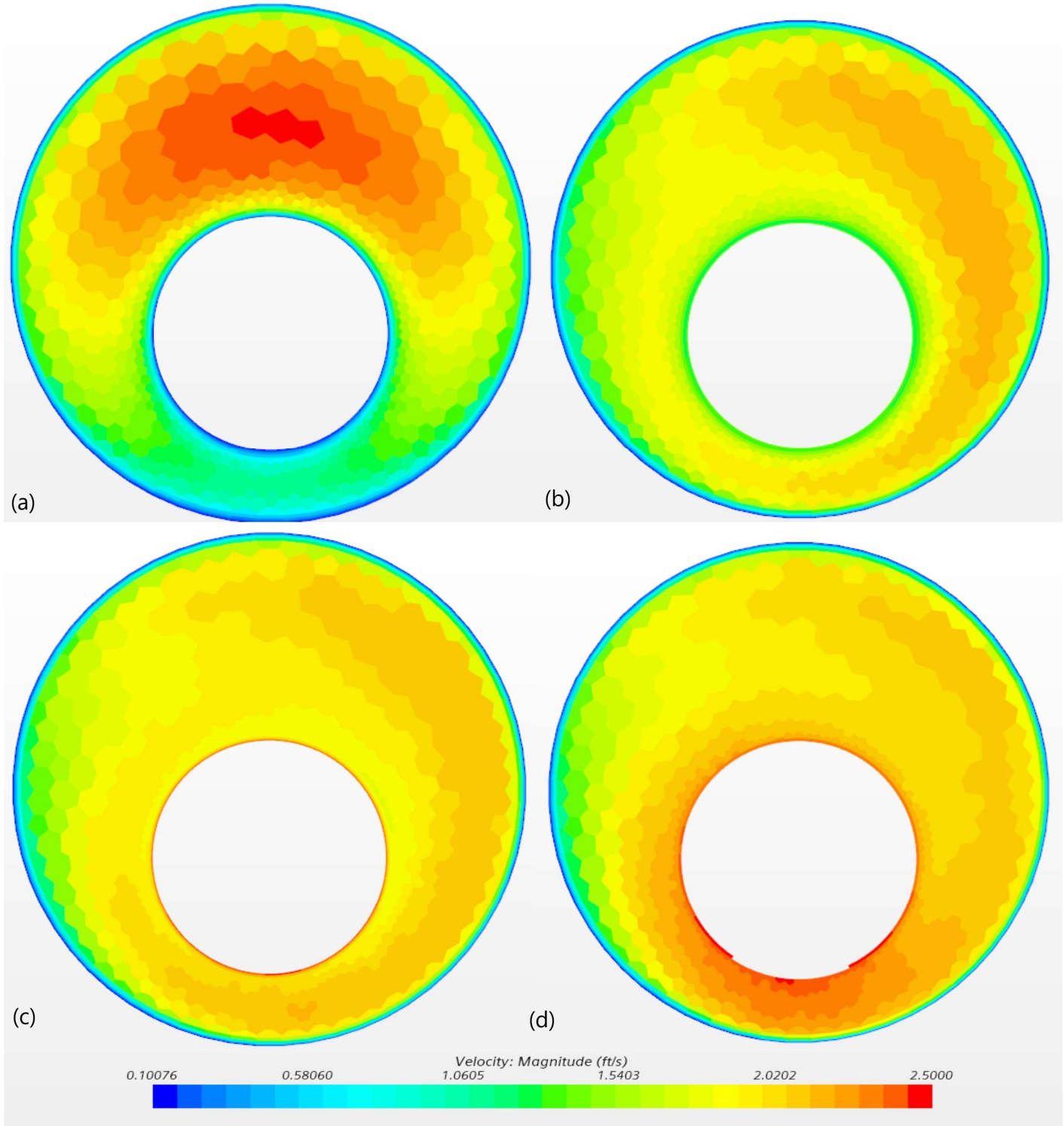

Figure 9:Cross-sectional analysis of flow channel development based on pipe rotation speed, absolute velocity magnitude (100 fpm linear velocity [500 gpm flow rate], bottom eccentric annulus, LWBM) (a) 0 RPM (b) 60 RPM (c) 120 RPM (d) 180 RPM

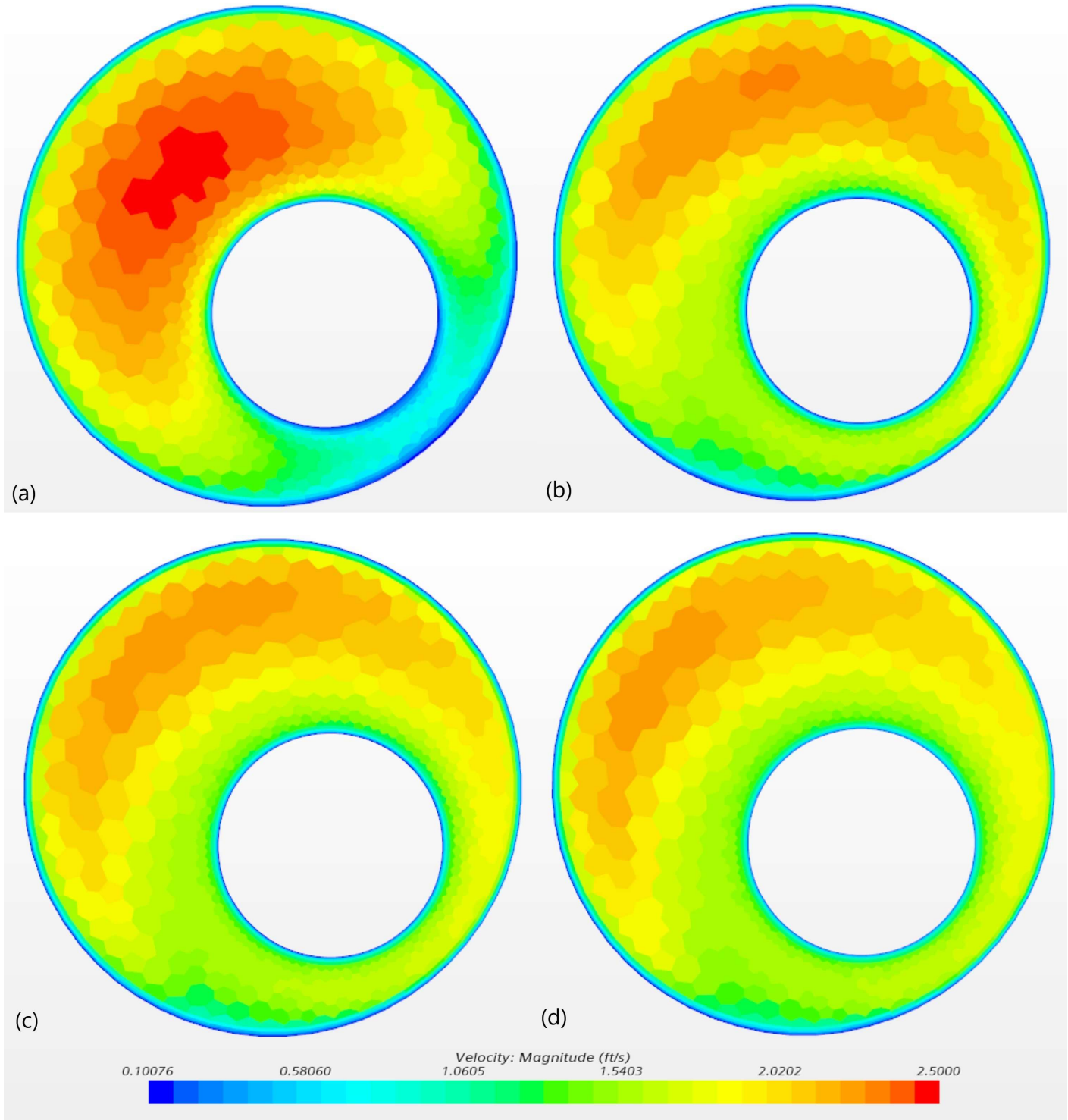

Figure 10:Cross-sectional analysis of flow channel development based on pipe rotation speed, velocity magnitude normal to inlet (100 fpm linear velocity [500 gpm flow rate], offset eccentric annulus, LWBM) (a) 0 RPM (b) 60 RPM (c) 120 RPM (d) 180 RPM

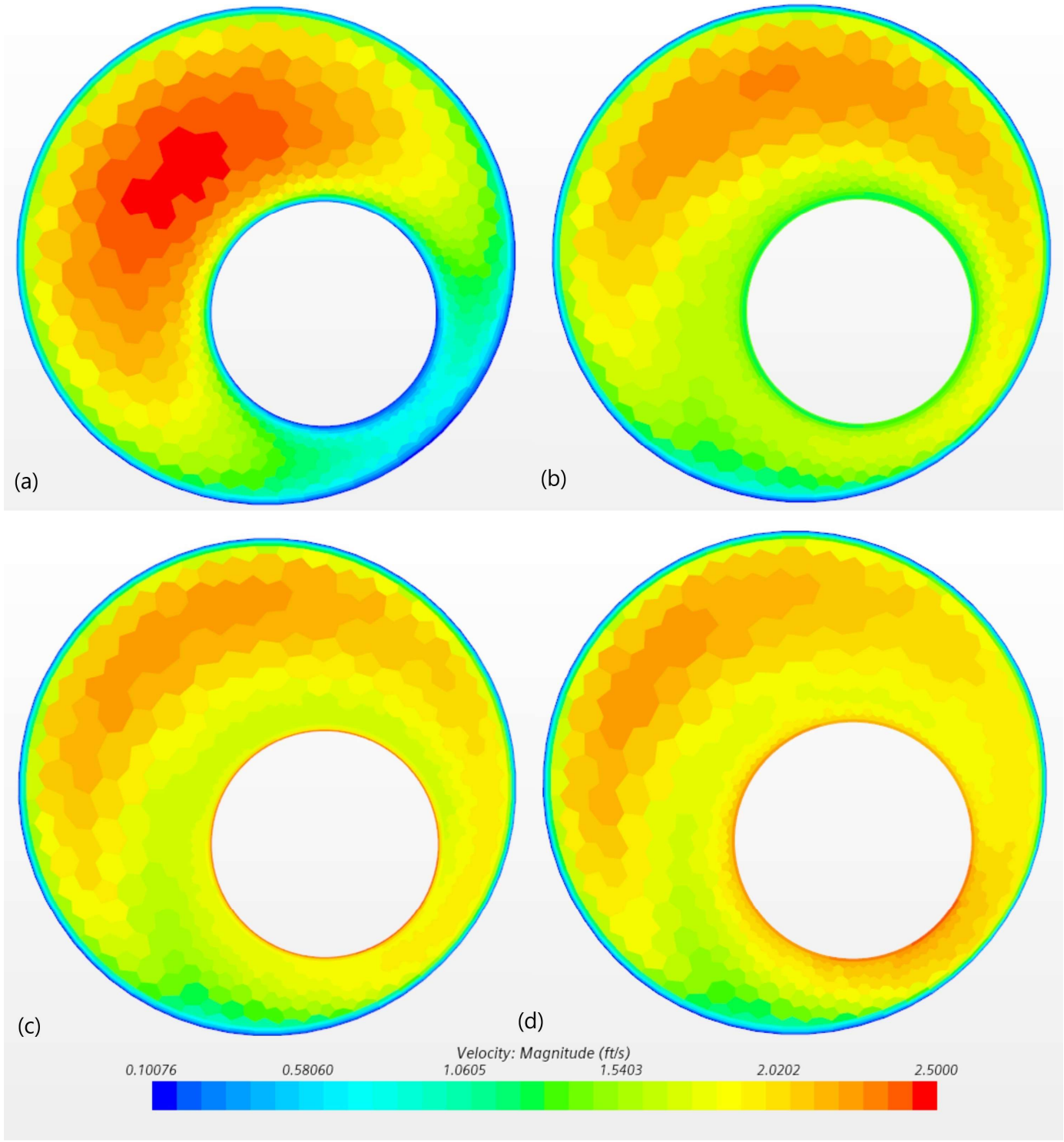

Figure 11:Cross-sectional analysis of flow channel development based on pipe rotation speed, absolute velocity magnitude (100 fpm linear velocity [500 gpm flow rate], offset eccentric annulus, LWBM) (a) 0 RPM (b) 60 RPM (c) 120 RPM (d) 180 RPM

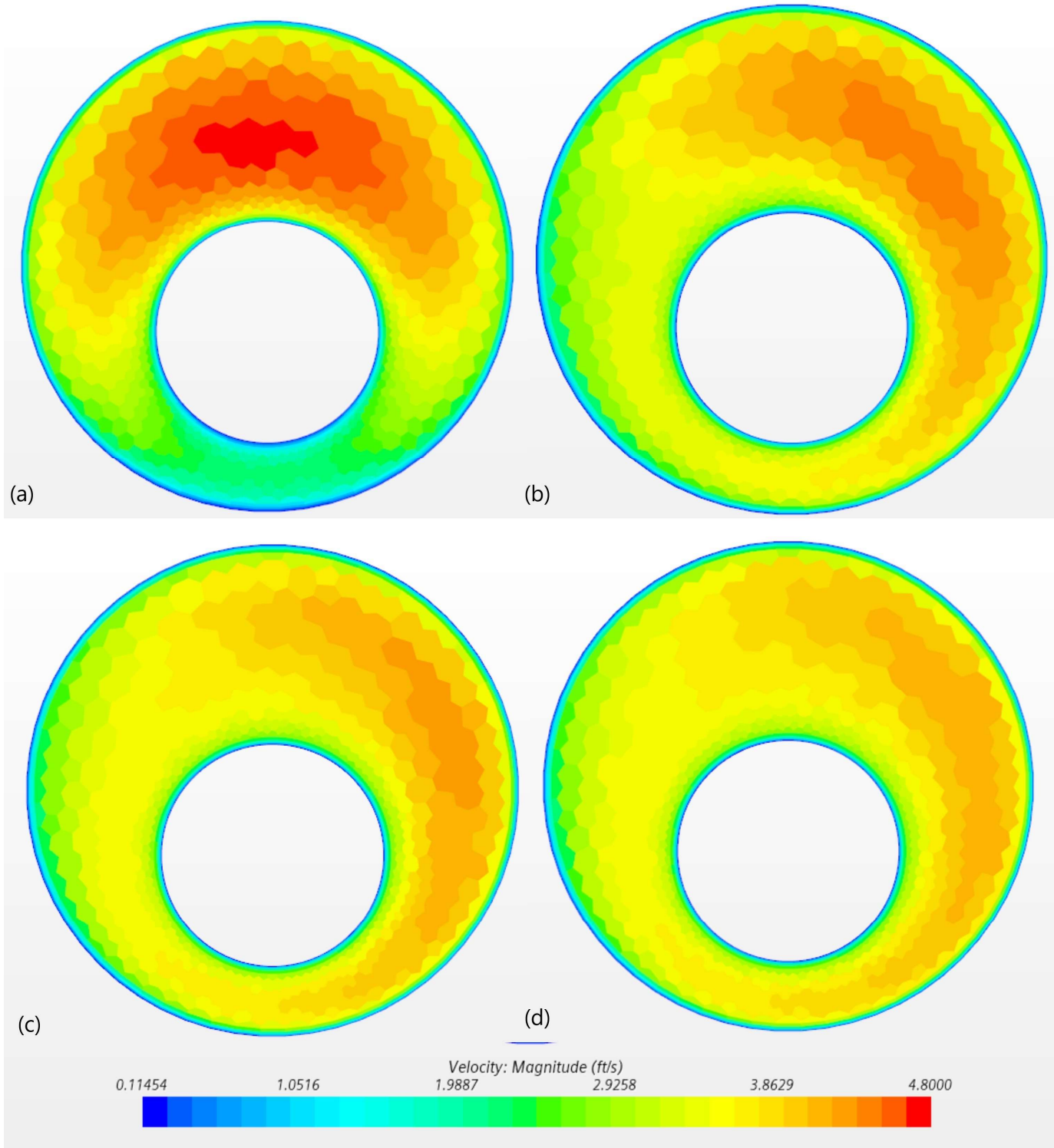

Figure 12:Cross-sectional analysis of flow channel development based on pipe rotation speed, velocity magnitude normal to inlet (200 fpm linear velocity [1,000 gpm flow rate], bottom-eccentric annulus, LOBM (a) 0 RPM (b) 60 RPM (c) 120 RPM (d) 180 RPM)

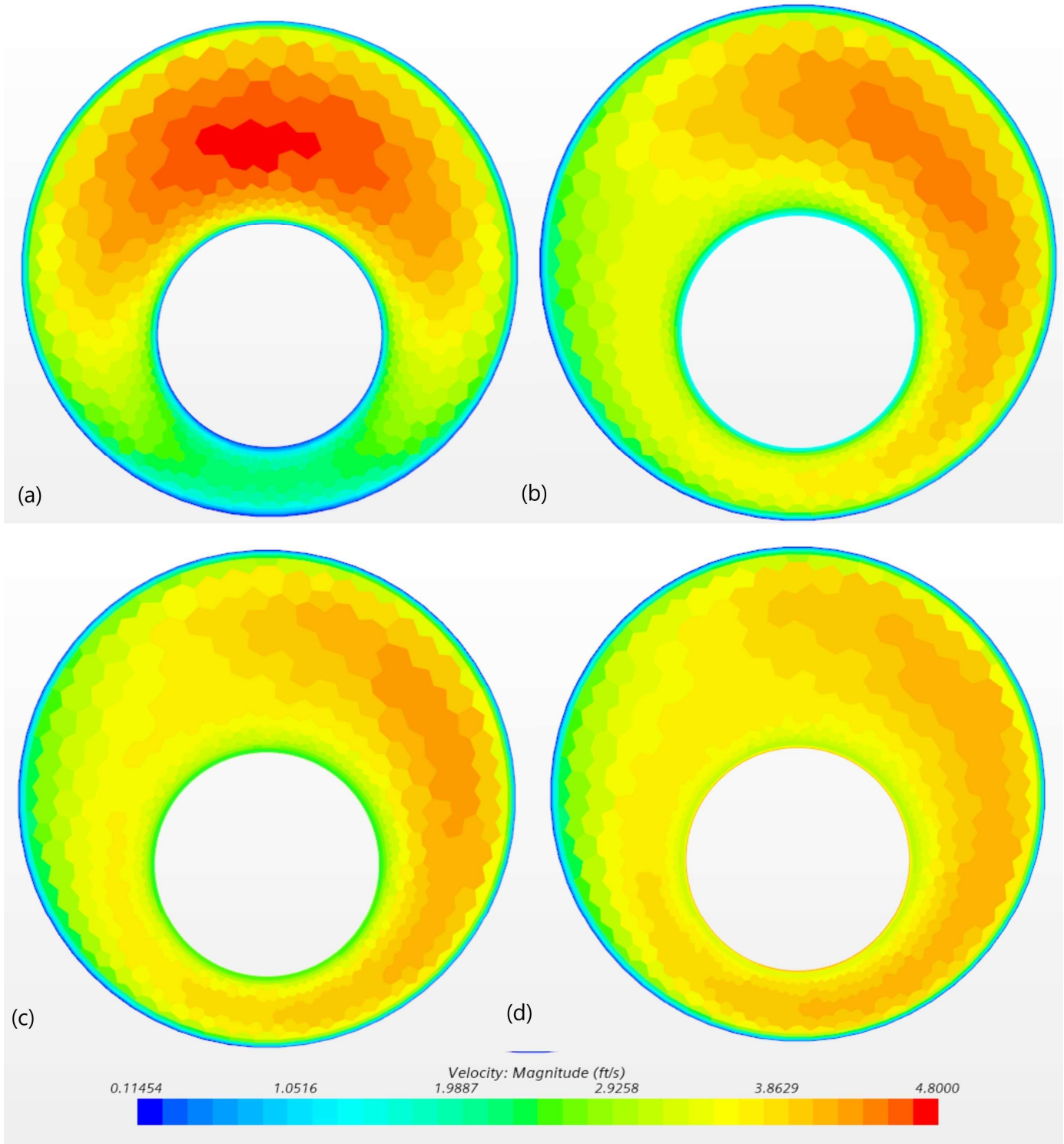

Figure 13:Cross-sectional analysis of flow channel development based on pipe rotation speed, absolute velocity magnitude (200 fpm linear velocity [1,000 gpm flow rate], offset eccentric annulus, LWBM) (a) 0 RPM (b) 60 RPM (c) 120 RPM (d) 180 RPM

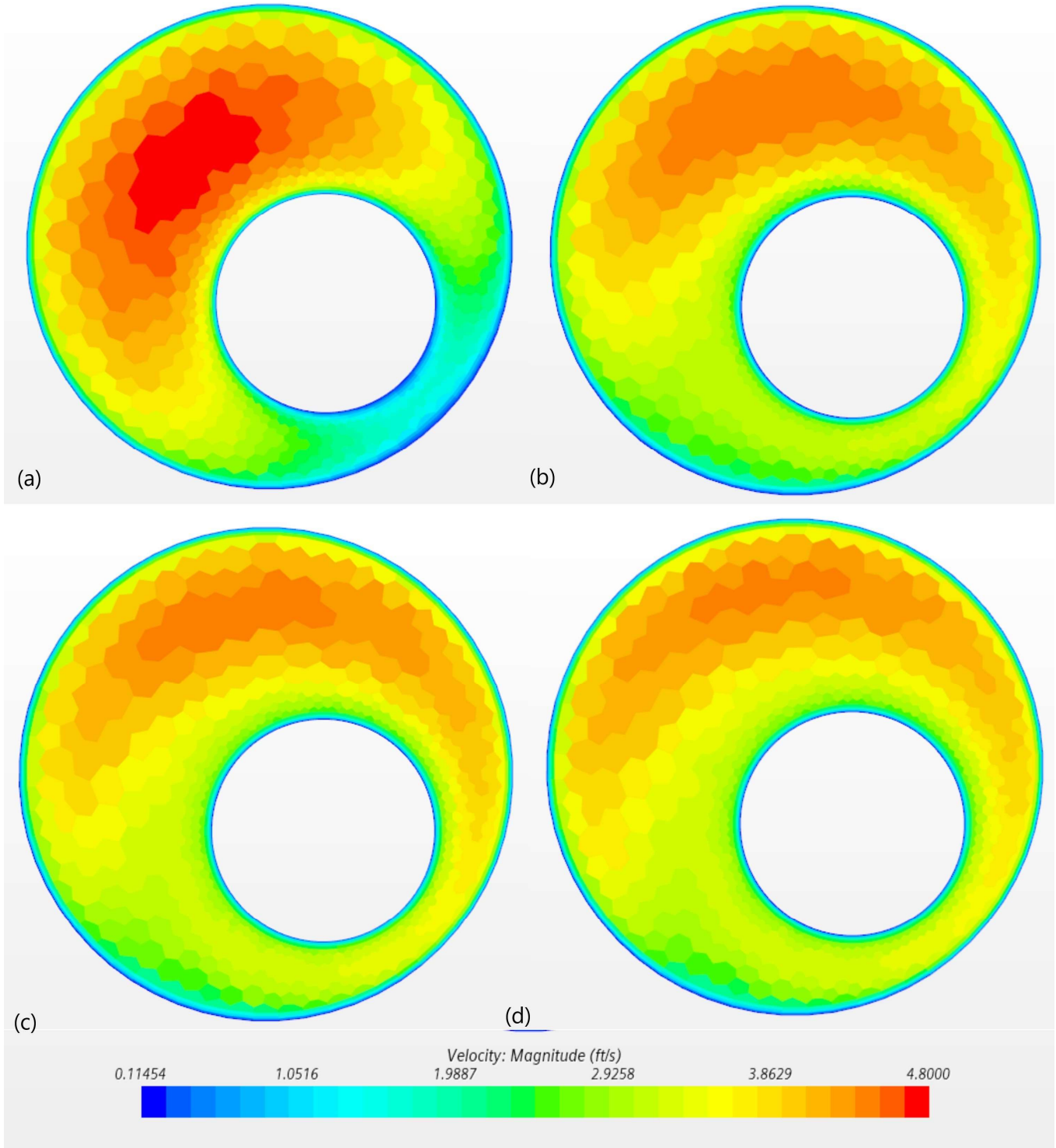

Figure 14:Cross-sectional analysis of flow channel development based on pipe rotation speed, velocity magnitude normal to inlet (200 fpm linear velocity [1,000 gpm flow rate], offset eccentric annulus, LOBM) (a) 0 RPM (b) 60 RPM (c) 120 RPM (d) 180 RPM

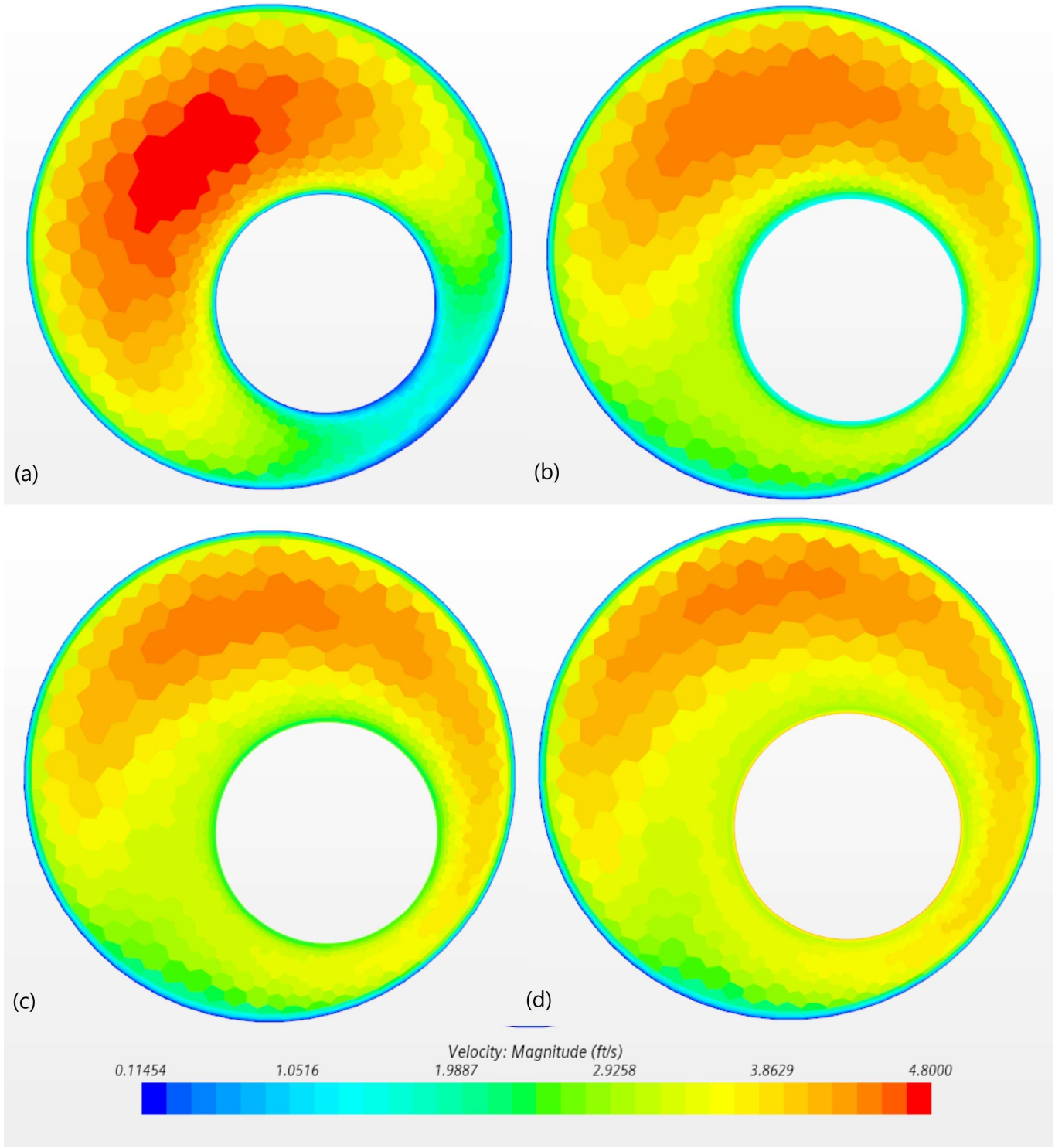

Figure 15:Cross-sectional analysis of flow channel development based on pipe rotation speed, absolute velocity magnitude (200 fpm linear velocity [1,000 gpm flow rate], offset eccentric annulus, LOBM) (a) 0 RPM (b) 60 RPM (c) 120 RPM (d) 180 RPM

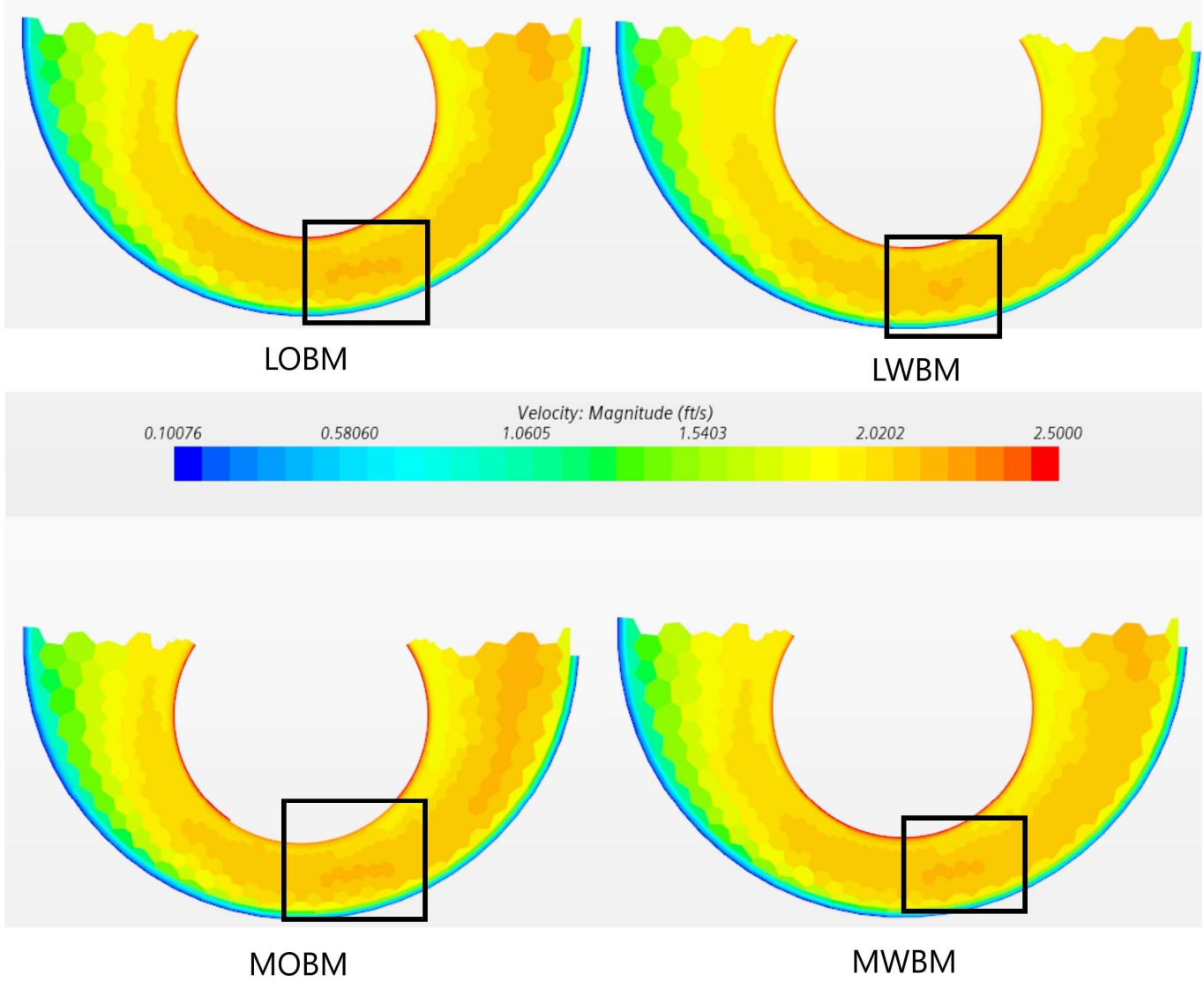

Figure 16:Cross-sectional analysis of secondary flow channel centroid at 120 RPM, absolute velocity magnitude (100 fpm linear velocity [500 gpm flow rate], bottom eccentric annulus)

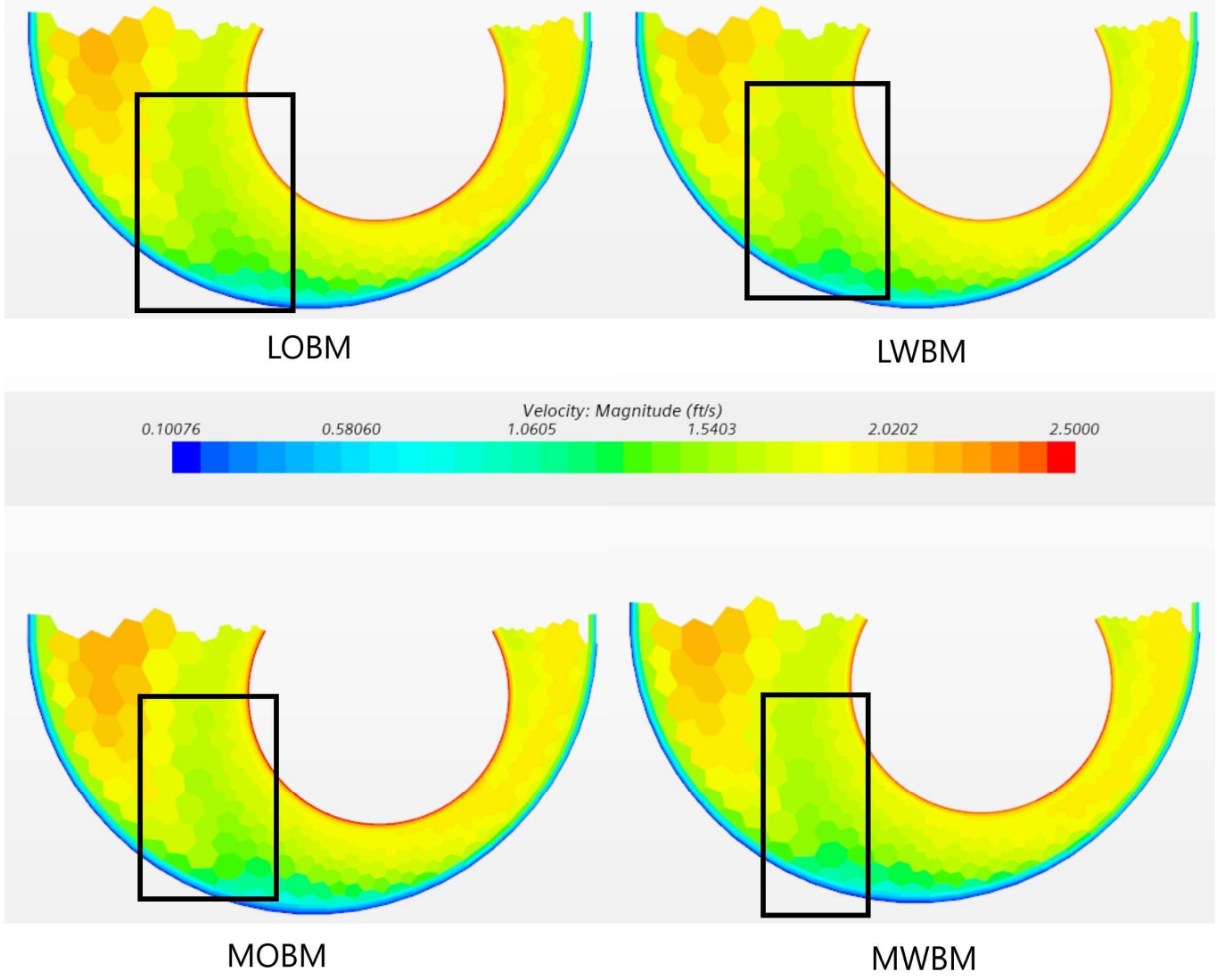

Figure 17:Cross-sectional analysis of flow channel cavity formation at 120 RPM, absolute velocity magnitude (100 fpm linear velocity, [500 gpm], offset eccentric annulus)